Conductance oscillations periodic in the density of one-dimensional electron gases

Stuart B. Field,* M. A. Kastner, U. Meirav, and J. H. F. Scott-Thomas
Department of Physics and Research Laboratory of Electronics, Massachusetts Institute of Technology, Cambridge, Massachusetts 02139

D. A. Antoniadis and Henry I. Smith
Department of Electrical Engineering and Computer Science and Research Laboratory of Electronics, Massachusetts Institute of Technology, Cambridge, Massachusetts 02139

S. J. Wind
IBM Research Division, Thomas J. Watson Research Center, P.O. Box 218, Yorktown Heights, New York 10598
(Received 26 March 1990)

Results are reported of a detailed study of the conductance oscillations in one-dimensional (1D) Si inversion layers. A comparison is made with results for GaAs accumulation layers. The conductance oscillates by as much as a factor of 100 and is accurately periodic in the number of electrons per unit length. The period varies randomly from sample to sample, and changes when a single sample is warmed to room temperature and remeasured at low temperature. Multiple periods are often observed, and the amplitude of the individual frequency components can be altered by moving the electron gas from side to side with a transverse electric field. These observations suggest that the period is determined by the distance between charged defects near the 1D channel. Measurements of the temperature dependence indicate that the oscillatory conductance reflects a periodic energy for a thermally activated conductance mechanism as well as a parallel oscillatory tunneling mechanism. The period of the conductance oscillations is found to be surprisingly independent of magnetic field B. However, the random modulation of the amplitude of the oscillations is reduced by a **B** field normal to the semiconductor surface, as it is by increasing temperature.

I. INTRODUCTION

In the late 1970's the rapidly improving theoretical description of disordered metals combined with the swiftly evolving technology of submicrometer lithography to create a new subfield of condensed-matter physics. The electronic properties of artificial structures which are large compared with atomic size scales but comparable to quantum-mechanical coherence lengths have been shown to be fundamentally different from both those of larger and of smaller structures. For this reason the term "mesoscopic" has been used[1] to differentiate them.

Almost from the start, the hallmark of mesoscopic structures has been the random, noise-like, but reproducible fluctuations in their conductance. These were first seen in the insulating regime of one-dimensional (1D) field-effect transistors when their Fermi energy was varied. The most dramatic discovery of this kind was that in metallic samples the fluctuations had magnitude of order e^2/h, independent of the size and geometry of the sample, in the limit of zero temperature. These universal conductance fluctuations, (UCF's) were seen when the magnetic field, Fermi energy, or impurity configuration was varied, consistent with the theory of Alt'shulter and of Lee and Stone.[2]

Recently we reported[3,4] the discovery of a new and different phenomenon in mesoscopic channels in semiconductors. In the same regime, where exponentially large random fluctuations had been seen in earlier devices,[2] we found fluctuations which, while still exponentially large, were accurately periodic in the density of the electron gas. Several models have been proposed to explain the observations. The purpose of this paper is to present the picture that has emerged from a very large number of experiments on one-dimensional channels in Si and to compare this picture with the predictions of the models. Some results for GaAs channels are also reillustrate the universality of the phenomena.

Our paper is organized in the following way: Section II provides a description of the structure and fabrication techniques for each device. Pertinent experimental details are also given there. In Sec. III we discuss semiclassical simulations of the potential and charge density for the device structures we have fabricated. Section IV provides the phenomenology. We show how the frequency of the oscillations varies from sample to sample, how the conductance evolves with temperature and magnetic field, and how the pronounced nonlinear dependence of the current on voltage is related to the oscillatory behavior. In Sec. V we compare the observations with the predictions of several models, and in Sec. VI we summarize our conclusions.

II. FABRICATION AND EXPERIMENTAL DETAILS

Results for two types of devices are discussed below. A dual-gate silicon metal-oxide-semiconductor field-effect transistor (MOSFET) with a novel split lower gate was

developed; this type of device has an extremely narrow electron gas ($\lesssim 30$ nm), and, for Si, a very high mobility. We also have fabricated narrow channels in GaAs/$Al_xGa_{1-x}As$ *inverted* heterostructures, which results in devices closely analogous to MOSFET's.

The details of Si MOSFET fabrication have been presented elsewhere,[5] and only a brief overview of the device geometry is presented here. Figure 1 shows a schematic cross section and a top view of the silicon device. Its unique feature is the refractory-metal lower gate with a 70-nm-wide slot, fabricated using x-ray nanolithography and liftoff. Note that the electron gas is much narrower than the slot in the gate as discussed below. This lower gate, held at a fixed voltage *below* inversion threshold, screens the electric field from the upper gate everywhere but under the slot. Only there can fields be high enough to create inversion and form a narrow electron gas. The density of this gas is varied by changing the upper-gate voltage V_G. An important fabrication step was a high-temperature anneal[5] which restored the high mobility lost during other fabrication steps.

The GaAs devices,[4] shown schematically in Fig. 2, are notable for their unique inverted semiconductor-insulator-semiconductor (ISIS) heterostructure.[6] A high-mobility electron gas is formed on *top* of the $Al_xGa_{1-x}As$ layer, and its density is controlled by the voltage applied to the degenerate *n*-type GaAs substrate. This allows variation of the carrier density over a wide range, which is not achieved in conventional GaAs modulation-doped structures. The narrow channel itself is defined by a gap in a shallow *p*-type implant.[4,7] The gap, patterned by electron-beam lithography, is 1.0 μm wide, but the electron channel was found to be much narrower; we estimate it to be about 70 nm.

The characteristics of both types of devices, which are summarized and compared in Table I, require some explanation. For the GaAs devices the Hall mobility was

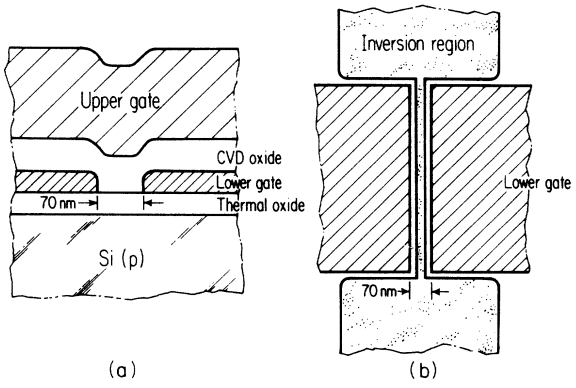

FIG. 1. Schematic (a) cross section and (b) top view of the silicon slotted-gate device. The width of the narrow region is exaggerated in (b). The inversion layer, formed by the positively biased upper gate, is confined by the lower gate. The thermal oxide and refractory-metal lower gate are both 30 nm thick. A similar device has been built in *n*-type silicon to study a one-dimensional gas of holes.

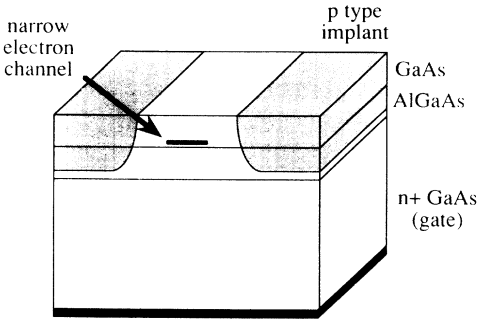

FIG. 2. Schematic of the GaAs device, which is an inverted heterojunction structure in which the density of electrons is controlled by the degenerate *n*-type GaAs gate. The electrons are confined laterally by acceptors implanted in the GaAs and $Al_xGa_{1-x}As$ layers.

measured on two-dimensional devices; for the Si devices the field-effect mobility was measured on much wider (but otherwise identical) devices, where the width is well known. The mobility is not independent of density, although the values quoted, which are the maxima, are valid for a wide range of densities.

The transport properties of the narrow silicon MOSFET's and the narrow GaAs ISIS's were measured in a dilution refrigerator at temperatures as low as 50 mK. Magnetic fields up to 8 T were available at these temperatures, and to 11 T at 450 mK in a separate pumped He^3 refrigerator. Great care was taken to eliminate any voltage noise which might heat the electrons at low temperatures; we estimate that such noise was reduced to below 5 μV rms. The highest possible electron temperature resulting from heating by this noise is given by $kT=eV$, or about 60 mK. In general, we measured the conductance of the narrow electron gases using conventional ac lock-in techniques while slowly changing the carrier concentration in the channel by sweeping the gate voltage V_G. For studies in the Ohmic regime the excitation (drain-source) voltage V_{DS} was kept less than kT/e to obviate heating, and the resulting ac current I was measured using a current amplifier with noise corresponding to 2×10^{-12} A (rms). For these low values of V_{DS} the conductance was found to be independent of V_{DS}. Identical, albeit noisier, results were found with dc measurements. The data do not depend on the sweep rate of the gate voltage, for rates less than 0.05 V/min.

III. SIMULATION

Simulations of the devices described in this paper were performed with the PISCES–IIB (Ref. 8) computer program. This program models both the electrostatic and steady-state behavior of semiconductor devices. It is semiclassical, in the sense that the carrier distributions obey Fermi-Dirac statistics, and the dispersion relation is assumed parabolic with the appropriate effective mass. However, the charge is treated as a classical continuum, equivalent to the Thomas-Fermi approximation. PISCES–IIB solves Poisson's equation and the hole and electron continuity equations self-consistently, for a

TABLE I. Summary of typical parameters for n-type channels in Si and GaAs. The large difference in capacitance and voltage range for occupancy of a single subband results from the variation of the voltage on the (upper) gate with the smaller capacitance in the case of the Si devices, but the variation of the voltage on the (substrate) gate with the larger capacitance in the case of GaAs.

Parameter	Silicon MOSFET	GaAs ISIS
4-K mobility ($cm^2/V\,s$)	15 000	300 000
Width (nm)	25	70
Lengths (μm)	1,2,10	2,8
Capacitance (pF/cm)	0.3	3
Effective mass m^*/m	0.19	0.067
Typical subband spacing (meV)	6	2
V_G range for single subband (mV)	1500	25

user-defined two-dimensional cross section of electrodes, semiconductors, and insulators. The differential equations are solved numerically on a discrete set of points. The Fermi-Dirac distributions are taken at a low but finite temperature, where the electrostatistics are virtually independent of temperature. The parameters used in the simulation, such as the thickness of layers and lithographic widths, were measured during fabrication to an accuracy of $\sim 10\%$.

The simulation performed on the silicon MOSFET was used to obtain several important device characteristics. The effective width of the electron gas was estimated by the full width at half maximum (FWHM) of the electron concentration for a case in which the channel was well inverted. The value of 30 nm, obtained this way, agreed to within 20% with the value obtained by measuring the transconductance of the device at 77 K and comparing it with the transconductance of a wide device. The width of the electron gas was independent of gate voltage (to 10%) over ranges much larger than those swept during the experiments.

Laux and Stern[9] carried out a more sophisticated calculation for an electrode structure very similar to ours. Solving Poisson's and Schrödinger's equations self-consistently, they determined subband energies as well as charge densities as a function of gate voltage. Scaling their results for the differences in electrode spacings, we estimate that for the parameters used in our experiments, only the first one or two subbands are occupied. It is important to note that the calculations of Laux and Stern, like our semiclassical simulations, indicate that the electron density in the channel is nearly proportional to the voltage on the upper gate.

The electron gas could be shifted laterally in the channel by biasing the two lower gates to different voltages. This effect was simulated and the amount of shift was ~ 10 nm/V between the two lower gates. Also, the effective width of the electron gas was much more sensitive to changes in the lower-gate voltage than to changes in the upper gate. For the data presented in this paper the undergate voltage was in the range 0.0–0.6 V.

Figure 3 shows the charge per unit length as a function of voltage on the upper and lower gates; the slopes give the capacitances. The ratio of the two capacitances is 10 ± 3. The value of the capacitance (between upper gate and channel) given in Table I is about 3 times larger than that quoted previously.[3] We have discovered that the earlier result was an error resulting from a false convergence. This, in turn, was caused by unfortunate choices of the size of the grid of points and of the size of voltage steps used in the simulation. The result quoted in Table I is independent of these sizes.

Similar simulations were done for the GaAs ISIS channels, which took into account lateral spreading (straggle) of the p-type implant that defined the channel. A detailed account of the results was given previously.[4] The most important finding was the dependence of the electron concentration on gate voltage, from which we derived the effective capacitance per unit length, $C \approx 3$ pF/cm. The simulation also produced the profile of the

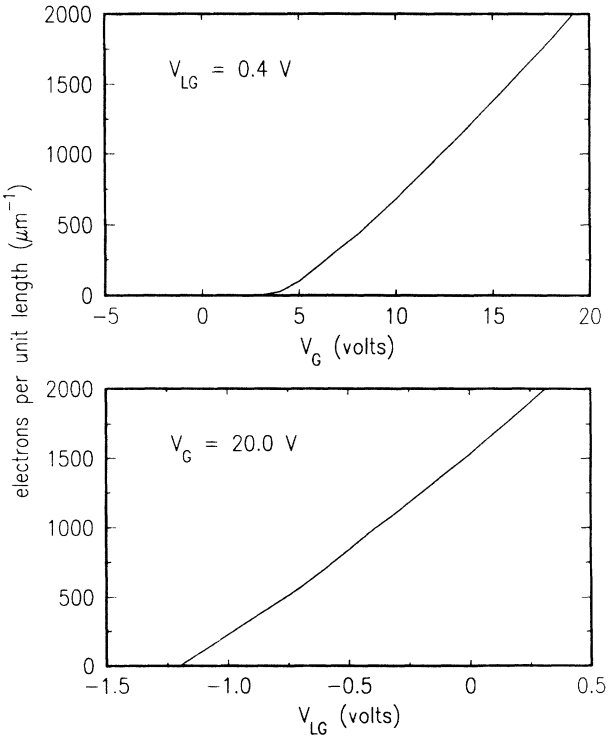

FIG. 3. Electron linear density as a function of bias on the upper gate (top panel) and lower gate (lower panel) for the Si slotted-gate device, as calculated by the program PISCES-IIB. Note the change of voltage scales.

laterally confining potential, which was found to be approximately parabolic at threshold. The energy spacing between the lowest one-dimensional subbands was estimated to be about 2 meV, giving a range of a few tens of meV in V_G where only the lowest subband was occupied. Finally, the width of the electronic wave function in the lowest subband was estimated to about 70 cm.

IV. PHENOMENOLOGY

A. General behavior of narrow channels

Figure 4 shows a typical example of the periodic conductance oscillations we have seen in the double-gate Si n-type-layer devices. The conductance varies periodically by orders of magnitude near threshold. As the electron density is increased by raising V_G, the minima increase more rapidly than the maxima; thus the oscillations disappear at high V_G. All the variations in conductance, both the periodic and randomly fluctuating components, are completely repeatable when V_G is ramped up and down.

The Fourier power spectrum is also shown in Fig. 4; the large, narrow peak corresponding to the periodicity of the oscillations is evident. The peak in the Fourier transform at zero frequency comes from two effects: First, the general increase of the maxima with V_G gives low-frequency Fourier components. Second, the random variation in the height of the maxima gives a broad peak at zero frequency, the correlation function of the random fluctuations. This random amplitude also broadens the peak that comes from the periodic oscillations. There are, in addition, smaller peaks in the Fourier transform corresponding to secondary frequencies that are not harmonics of the primary one. Figure 5 shows that the oscillations can be remarkably periodic.

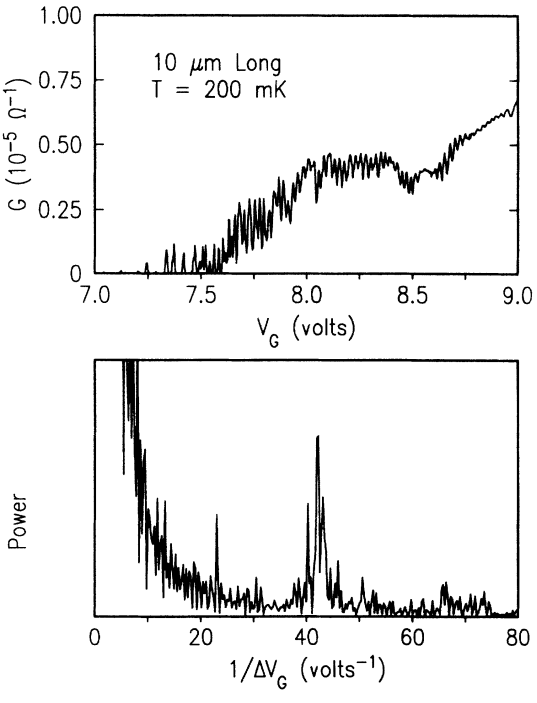

FIG. 4. Conductance G vs V_G for a 10-μm-long inversion layer in silicon (upper panel) and the Fourier power spectrum of the same data (lower panel).

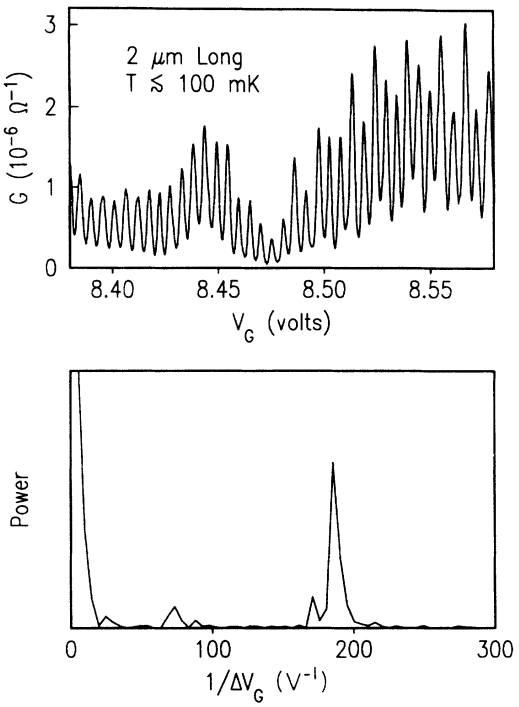

FIG. 5. G vs V_G and Fourier transform for the highest-frequency oscillations yet observed in Si n-type-channel devices.

Figure 6 shows the same phenomena in a GaAs ISIS device. The inset shows that near threshold the oscillations correspond to periodic sharp peaks in the conductance. Figure 7 shows conductance oscillations in a Si p-type layer. Whereas Figs. 4–7 indicate that the oscillatory behavior is quite general, it is important to remember that it was not observed in earlier narrow MOSFET's,

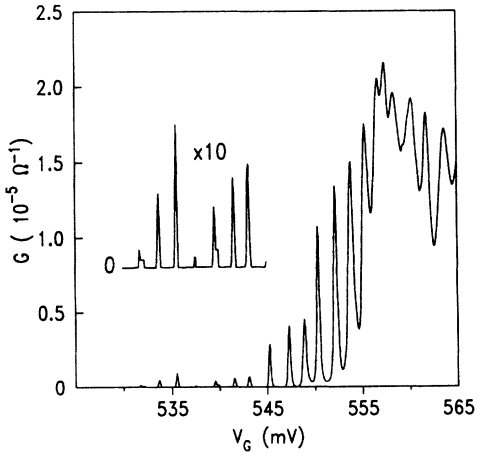

FIG. 6. G vs V_G for a 2-μm channel in a GaAs device, measured at $T = 50$ mK. The inset shows an expansion of the oscillations close to threshold.

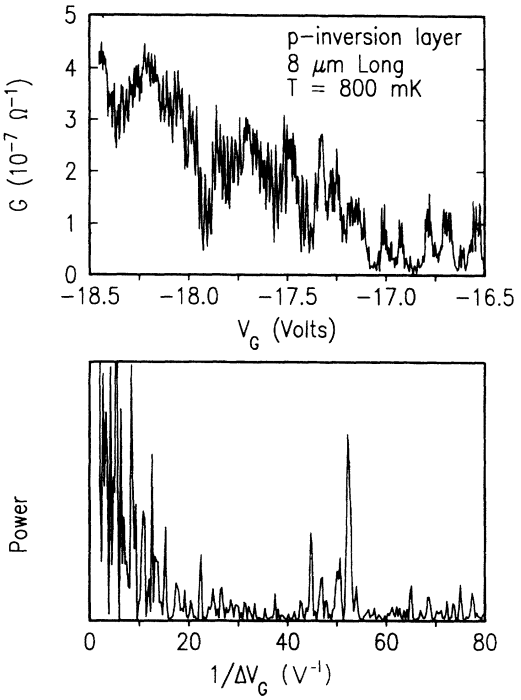

FIG. 7. G Vs V_G for an 8-μm-long inversion layer in n-type silicon (upper panel) and the Fourier spectrum of the data (lower panel). The carriers are holes in this case, and the gate must, therefore, be biased negatively.

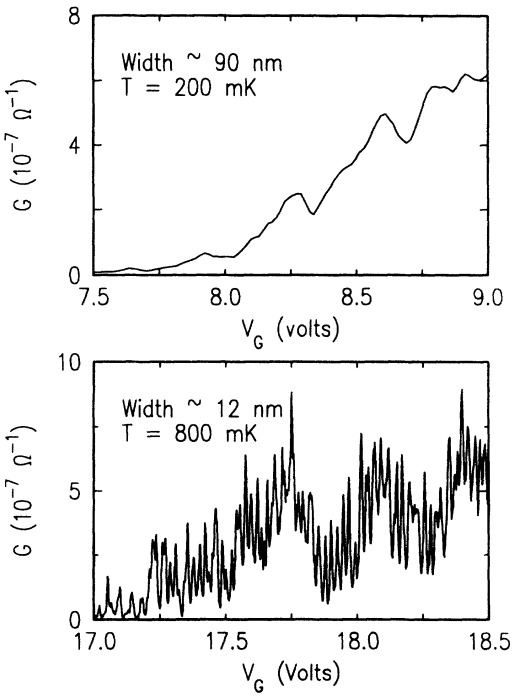

FIG. 8. G vs V_G for a silicon device in which the effective width of the electron gas is 90 nm (upper panel). The slope of the conductance increases by a factor of ~6 for larger gate voltages than those shown. The lower panel shows the same measurement on a device with a narrower effective width (~12 nm) on the same wafer. The threshold for the latter is larger because the upper gate must overcome the fringing fields of the lower gate.

which were wider or had lower mobility, or both.[2] Figure 8 shows a comparison of two n-type inversion layers of different widths on a wafer whose two-dimensional (2D) field-effect mobility was measured to be 10 000 $cm^2/V\,s$. The channel width estimated from the conductance is 12 nm for the one that shows periodic oscillations; the 90-nm-wide channel shows no oscillations. All Si double-gate structures with width less than 30 nm have shown the oscillations. This is not the case for the GaAs devices. Only about 30% of devices such as the one for which data are shown in Fig. 6 show the periodic oscillations.

B. Sample-to-sample variation of the frequency of oscillation

In a previous publication[3] we showed that the period varies randomly from sample to sample. This is illustrated in a different way in Fig. 9, where we show the conductance for channels of different length on the same wafer. Indeed, the frequency changes even for a single device when cycled from low temperature to room temperature and back again. In Fig. 10 are two sets of data for the same 10-μm-long sample. Each set was completely reproducible over a period of weeks, as long as the sample was kept at low temperatures. The two sets were taken in different runs separated by 6 months, and the sample was brought to room temperature in the interim. Similar behavior was seen for the GaAs devices. For example, the device of Fig. 6 showed no oscillations after temperature cycling. Because the frequency of oscillation changes randomly from sample to sample and for the same sample when the temperature is cycled, we proposed that the frequency is determined by the position of charged defects or impurities near the semiconductor-insulator interface.

Ancillary evidence for this comes from an experiment that takes advantage of the unique features of the dual-gate Si device. Because the lower gate has a gap, one can

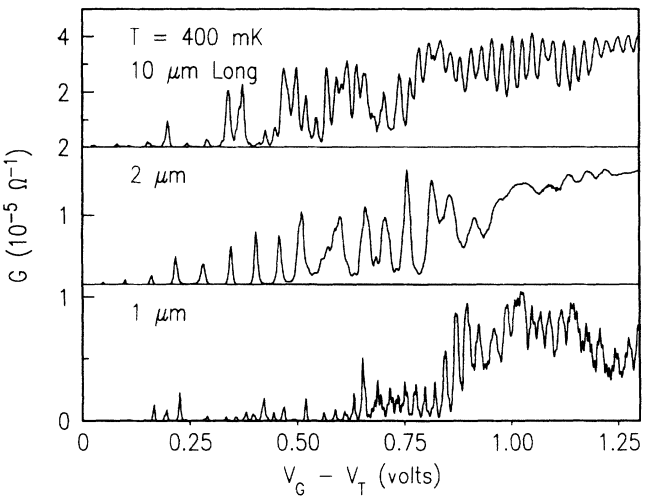

FIG. 9. G vs V_G for Si devices with 10-, 2-, and 1-μm-long regions, respectively, from top to bottom. The period is not related to the length of the device.

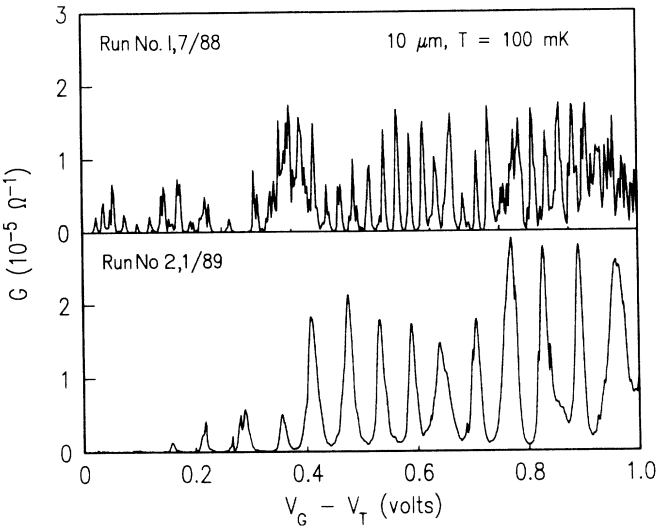

FIG. 10. Two measurements of G vs V_G performed on the same 10-μm Si device, cycling the device to room temperature and back to 100 mK between measurements. The data in the top panel were taken 6 months before those in the lower panel.

apply a voltage difference between the two halves, which shifts the center of charge of the channel to the left or right, as discussed in Sec. III. Figure 11 shows the results of such an experiment. With the two halves of the split gate at the same potential (center bias), this device shows two frequencies, one with $\Delta V = 5.4$ mV and the other with $\Delta V = 65$ mV. Of order 100 periods of the higher-frequency oscillation can be observed. When the split gate is biased to shift the electrons in the channel to one side (arbitrarily labeled left), the high-frequency component almost disappears. When the electrons are shifted to the right, the low frequency is suppressed more than the high one. This suggests that the frequency is determined by potential fluctuations caused by defects or impurities near the channel and that the effect of the electric field transverse to the channel is to increase or decrease the interaction of the inversion-layer electrons with those potential fluctuations. It is surprising that the simulation discussed in Sec. III predicts a shift of the charge in the channel by only ~ 3 nm for the voltage difference between the two halves of the gate used for the experiment of Fig. 11. This may be a case in which more sophisticated modeling like that of Laux and Stern[9] is necessary.

As discussed in Sec. III, the capacitance between the channel and the lower gate is much larger than that between the channel and the upper gate. To check our simulations and the hypothesis that the oscillations result from the variation of electron density in the channel, we measured the conductance as a function of voltage on each gate. The conductances and Fourier transforms are shown in Fig. 12. The ratio of the frequencies is 12, in

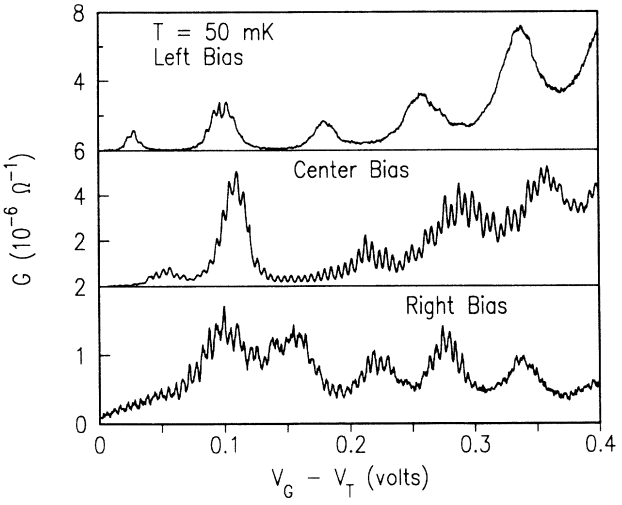

FIG. 11. Two oscillatory components of conductance change in relative amplitude as the relative bias on the two halves of the lower gate is changed. The voltage between the two halves for left and right bias is ± 0.45 V. Changing the relative bias shifts the position of the electron gas laterally, so that the impurity potential felt by the gas is different.

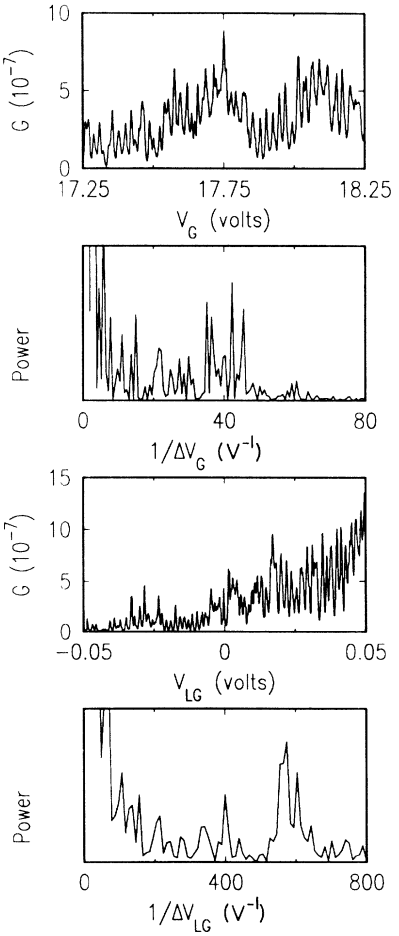

FIG. 12. The top two panels show conductance oscillations and Fourier transform as the *upper gate* is swept. The lower two panels show the oscillations and Fourier transform for the same device, but sweeping the *lower gate* and holding the upper-gate voltage constant. Note that the frequency differs by about a decade.

good agreement with the value for the ratio (10±3) from the simulation.

C. Temperature dependence

The amplitude of the conductance oscillations decreases as the temperature is raised. An example of this is shown in Fig. 13 for gate voltages near threshold where, at the lowest temperature, the conductance varies periodically by more than an order of magnitude. In this example, as in Fig. 11, two frequencies are evident. As the temperature is raised, both maxima and minima increase in conductance, but the minima increase faster causing the oscillations to disappear. Figure 14 shows that the conductance is thermally activated. We have extracted the approximate activation energy as a function of V_G from data like those in Figs. 13 and 14 and have plotted it along with the conductance itself in Fig. 15. This shows that the oscillatory conductance results, at least at relatively high temperature, from periodic oscillations in the activation energy.

The amplitude of the periodic activation energy is not correlated with the frequency of oscillations from one sample to another. For example, Fig. 16 shows the activation energy as a function of V_G for two devices whose 2D mobilities and estimated widths are given in the caption. Whereas the maximum activation energies differ by almost a factor 10, the frequencies are almost the same.

At the lowest temperatures the conductance becomes independent of T, but it still oscillates periodically with V_G. The T-independent conductance persists to 300 mK in the GaAs channels, a temperature much higher than the maximum temperature that can be accounted for by electron heating (see Sec. II). Figure 17 shows the temperature dependence for such a channel. As pointed out previously,[4] this is strong evidence for a tunneling component which oscillates in phase with the activated component.

One last feature of the temperature dependence is

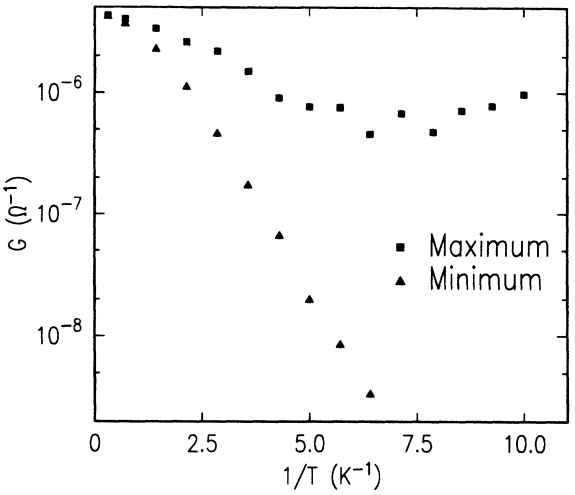

FIG. 14. G vs T^{-1} for a maximum and a minimum in the conductance of a Si n-type channel on a semilogarithmic scale. The conductance is activated at the minimum. The maximum is temperature independent when T is low enough, and has a weak T dependence, corresponding to a small activation energy at high T.

demonstrated by Fig. 18, which shows the conductance of one device over a broad range of gate voltage at temperatures between 100 and 800 mK. The random modulation of the conductance disappears more rapidly with increasing T than does the periodic component. However, as seen also in Fig. 13, the frequency of the oscillations is temperature independent.

D. Magnetic field dependence

Although the random modulation of the conductance is reduced by a magnetic field as it is by increased temperature, the periodic component is remarkably unaffected. Figure 19 shows how the conductance evolves up to $B = 8$ T for the field applied normal to the (100) surface of the Si wafer. Between 0 and 3 T the mag-

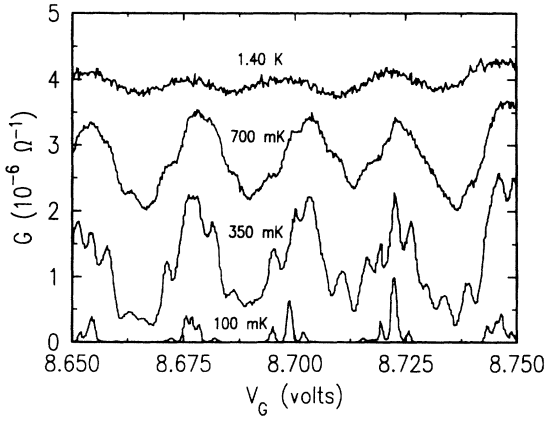

FIG. 13. Conductance oscillations with two different periods can be seen in this 10-μm Si device. As the temperature is increased, the conductance rises at the minima more rapidly than at the maxima.

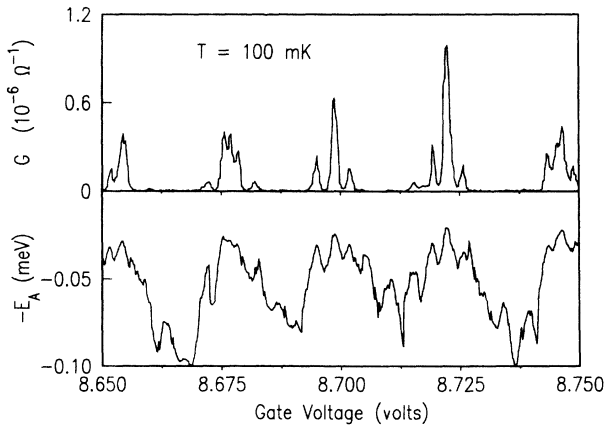

FIG. 15. The conductance (upper panel) and negative of the activation energy (lower panel) as a function of V_G. The conductance oscillations at high T are the result of oscillations of the activation energy.

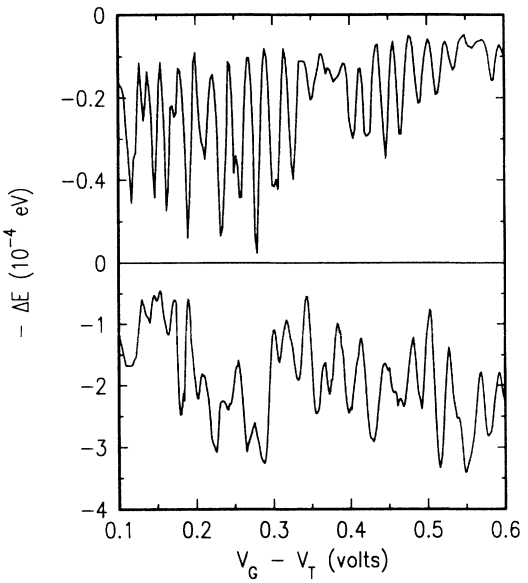

FIG. 16. The activation energy as a function of gate voltage (relative to threshold) is compared for two devices having almost the same period of oscillations. The maximum activation energies differ by almost a factor 10. The device in the upper panel has an effective width of 30 nm and a 2D mobility of $\sim 15\,000\ cm^2/V\,s$; that in the lower panel has a width of ~ 12 nm and a mobility of $\sim 10\,000\ cm^2/V\,s$.

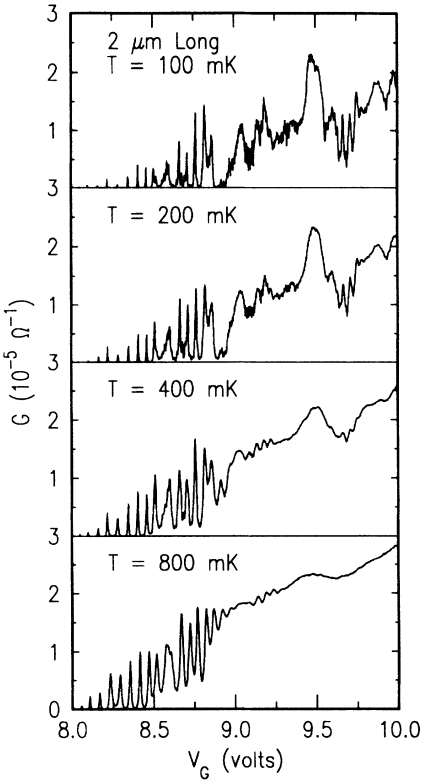

FIG. 18. Conductance oscillations at temperatures from 100 mK (upper panel) to 800 mK (lower panel) for the same 2-μm-long device. The period of the oscillations is temperature independent, but the random, nonperiodic fluctuations seen at 100 mK disappear with increasing temperature.

netic field drastically attenuates the random modulation. By contrast, from the data at higher field it is clear that the periodic component is unaffected. Small details in the structure, such as the double peak near 8.7 V, are preserved from 3 to 8 T; in particular, there is no evidence for splitting of peaks or periodic modulation of activation energies with increasing B.

Figure 20 shows that when the magnetic field is in the plane of the Si wafer and perpendicular to the 1D channel, the field again leaves the frequency of oscillations unchanged, in this case up to 11 T. The lowest panel shows the frequency, as determined from the Fourier transform, as a function of B. The reduction of the overall amplitude of the oscillations is dramatic for this orientation of B. Positive magnetoresistance was also measured for a 2D MOSFET on the same wafer, for the same field orientation. However, the fractional reduction of the conductance was only 20% in the 2D case.

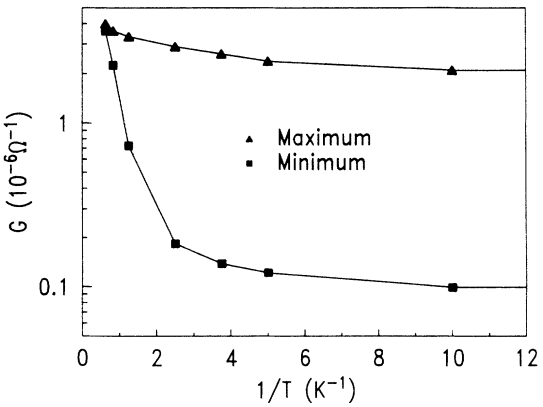

FIG. 17. G vs T^{-1} for a GaAs device at a minimum and a maximum on a semilogarithmic scale. Both show conductance below 250 mK that is temperature independent, suggesting a tunneling mechanism.

In Fig. 20 one can see that a high-frequency component emerges as B is increased. Figure 21 shows data taken with the data of Fig. 11, in which the inversion layer was shifted from side to side. The magnetic field (perpendicular to the Si surface) changes the relative strength of the two periodic components, as did the voltage between the two halves of the lower gate. This suggests that the enhanced confinement of the electrons in the magnetic field alters their interaction with the interface charges. For the case in which B is in the plane of the Si surface, the enhanced confinement brings the electrons closer to the interface, increasing their interaction with interface charges. This might explain the reduced conductance.

E. Non-Ohmic behavior

All the data discussed so far were measured with V_{DS}, the voltage along the 1D channel, small enough that the current I was proportional to V_{DS}. However, the oscilla-

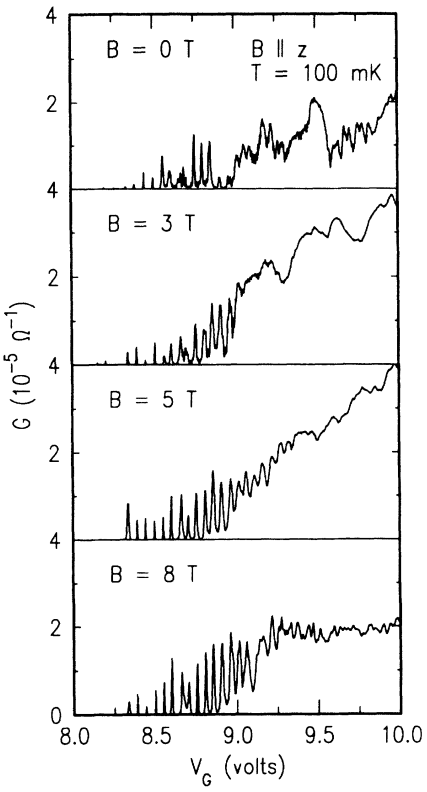

FIG. 19. Evolution of the conductance oscillations in a Si device as the applied magnetic field is increased from 0 T (upper panel) to 8 T (lower panel). The coordinate system used in Figs. 19–21 has $\hat{\mathbf{x}}$ in the direction of the electron gas, $\mathbf{z}$ perpendicular to the Si/SiO_2 interface. The magnetic field does not change the period, but does suppress the random fluctuations seen at 0 T.

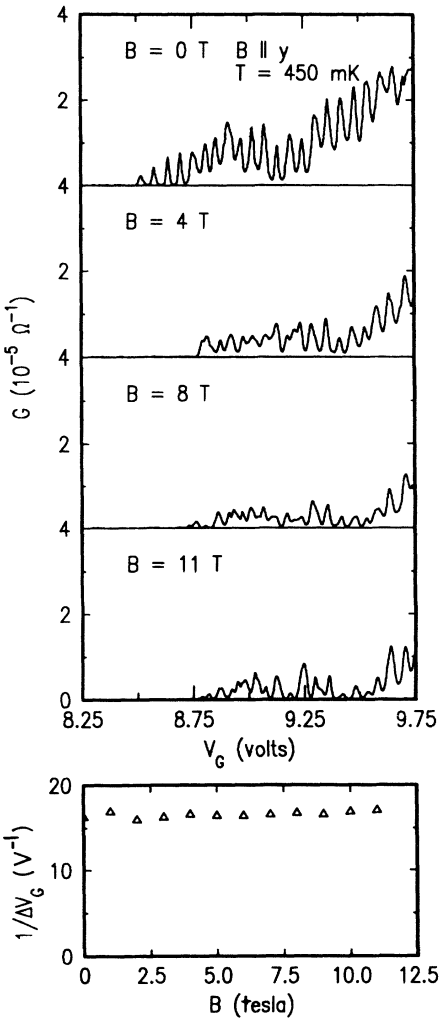

FIG. 20. The top four panels show the evolution of the conductance oscillations as B is increased from 0 T (top panel) to 11 T (fourth panel). The field is in the plane of the Si/SiO_2 interface, and perpendicular to the current. Again, the period does not change, although the overall value of the conductance is suppressed. The lowest panel shows the frequency of the peak in the Fourier spectrum as a function of the magnetic field; the frequency is independent of magnetic field.

tions are accompanied by dramatic nonlinearities in I at higher V_{DS}. The differential conductance dI/dV_{DS} is shown as a function of V_{DS} in the upper panel of Fig. 22 at a minimum in the Ohmic conductance versus V_G. In the second panel is the current-voltage characteristic that results from a numerical integration of dI/dV_{DS}. The high-voltage current extrapolates back to zero at $V_{DS}=0$, and obvious threshold behavior is observed. The behavior in the GaAs channels is much more complicated. For those, the differential conductance shows a great deal of structure near threshold, and does not typically extrapolate to $V_{DS}=0$.

Figure 22 illustrates threshold behavior in the I-V characteristic when V_G is held at minima in the Ohmic conductance. There is similar behavior at the maxima. Figure 23 shows, in the upper left panel, the Ohmic ($V_{DS}=50$ μV) conductance as a function of V_G over several periods of the oscillatory conductance. The data in this panel were taken at 800 mK so the conductance at both maxima and minima could be measured easily. The points marked 1 and 9 are the first and last of a sequence of gate voltages at which the differential conductance was measured as a function of V_{DS}; these nine sweeps are shown counterclockwise in the remaining panels. For the latter measurements the temperature was lowered to 100 mK to accentuate the non-Ohmic behavior. Beginning at a minimum (1) one sees a well-developed nonlinear characteristic with a large threshold voltage. As the peak conductance is approached (4 and 5), the threshold voltage shrinks, becoming so small that the conductance is finite even at $V_{DS}=0$. Finally, at the second minimum, the threshold voltage is large again. It is clear that there is pronounced nonlinearity at the maxima in the conductance, as well as at the minima, but it is also clear that the threshold value of V_{DS} oscillates with the conductance itself.

V. DISCUSSION

Using the values of capacitance per unit length C determined as described in Sec. III, we find that the ob-

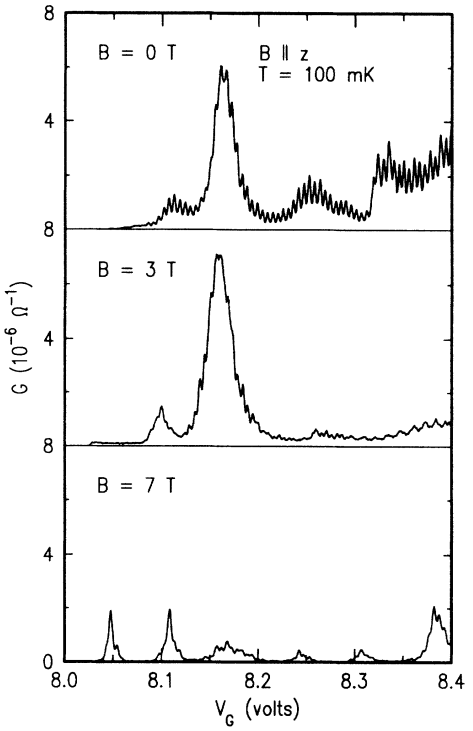

FIG. 21. G vs V_G for magnetic fields between 0 and 7 T directed normal to the Si/SiO_2 interface. For the top panel there is no applied field, and the oscillations with a high frequency are evident. As the magnetic field is increased, the magnitude of these decreases, and at 7 T a second, lower frequency is obvious.

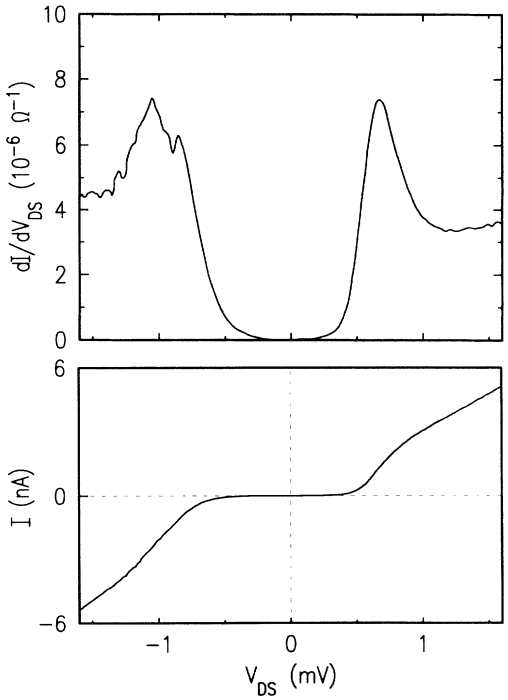

FIG. 22. The differential conductance vs applied source-drain voltage V_{DS} for a conductance minimum at $T=100$ mK (upper panel). The differential conductance is numerically integrated to give current vs voltage (lower panel). Extrapolation of the linear regions at high V_{DS} give a line passing through the origin.

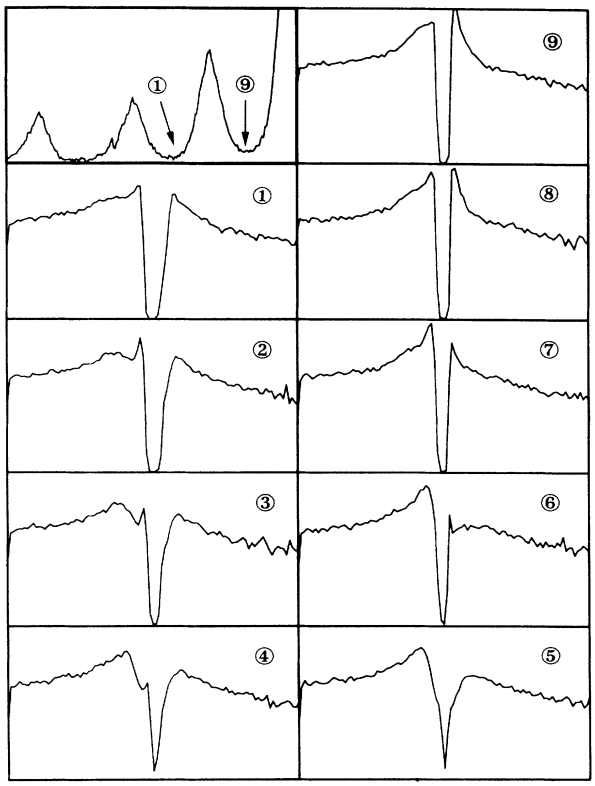

FIG. 23. The upper left panel shows conductance oscillations. The range of the horizontal axis is 9–9.2 V, and that of the vertical axis $(0-6)\times10^{-7}$ Ω^{-1} The next nine panels (labeled 1–9) show the differential conductance vs V_{DS} for different values of the gate voltage, beginning at the point marked 1 in the upper left panel, and ending at 9. V_{DS} ranges from -8 to 8 mV, and the differential conductance from 0 to 5×10^{-6} Ω^{-1}. The threshold for nonlinear conductance varies with the gate voltage, being largest at the minima and smallest at the maxima.

served period ΔV corresponds to a length per electron $L_0=(C\,\Delta V/e)^{-1}$, which falls in the range 0.1–1 μm. This is of the same order as the distance between the interface charges that happen to reside over the ~30-nm-wide Si channel, or the ~100-nm-wide GaAs channel. These charges are known to have densities of a few times 10^{10} cm^{-2} in our Si devices and a few times 10^9 cm^{-2} in the GaAs structures.[10] As discussed above, the evidence is very strong that it is such charges that determine L_0. It is less obvious, however, how the oscillatory phenomena come about.

A. Resonant tunneling of noninteracting electrons

It is incumbuant upon us to first explore whether a noninteracting-electron picture is adequate to explain the phenomena. One may assume that the charged impurities introduce barriers along the 1D channel which cause a segment to be approximately isolated. If the barriers are sufficiently high and wide, there will be sharp resonances in transmission when the Fermi energy coincides with one of the eigenstates of the isolated segment. This

coincidence will occur whenever the average charge in the segment corresponds to an odd multiple of $e/2$, resulting in a conductance that is periodic in the number of electrons per unit length.

There are, however, several observations that cannot be understood in this way. First, the degeneracies, twofold for spin, and a second twofold for valley in Si, would pin the Fermi energy at the single-particle levels. This would make the maxima wider than the minima, whereas the opposite is observed. Second, the magnetic field would lift the spin degeneracy, resulting in a splitting of the peaks. As seen from Figs. 15 and 16, we typically find activation energies $\Delta E \sim 0.1-1$ meV, but we have seen no spin splittings up to 11 T, which corresponds to energies of ~ 1 meV for $g=2$. Third, the single-particle energies would increase with wave vector k as k^2, at least at energies small compared with the barrier height, so that, although the spacing of the resonances in density would be expected to be constant, their spacings in energy, and therefore the activation energies at the minima, would be expected to grow with density. On the contrary, the temperature dependence becomes weaker for minima at progressively higher V_G. Fourth, the I-V_{DS} curve would display a series of steps, a new one for each resonance that falls between the Fermi levels of the two contacts, whereas we see only a single threshold. Last, the highest frequency we have observed in Si (the one seen in Fig. 5) gives L_0 close to the sample length $L=2$ μm. However, the twofold valley and twofold spin degeneracies and the requirement that the length of the isolated segment be less than L would require $L_0 < L/4$ for this simple resonant-tunneling model.

B. Coulomb blockade

It is, perhaps, not surprising that the simplest resonant-tunneling model is inadequate, because it ignores the electron-electron Coulomb interaction, which turns out to be a very large energy. The Coulomb-blockade (CB) model is the simplest one that incorporates these interactions.[11] Again, it is assumed that barriers isolate a subsection of the channel. It is further assumed that tunneling through the barriers is sufficiently slow that the charge in the isolated segment is quantized. Because of the electron-electron interaction, there is a cost in energy of adding extra charge to the segment. The CB model treats this interaction in mean-field theory, in which the energy cost to place charge Q on the isolated segment is just the classical energy for charging a capacitor, $(Q-Q_0)^2/2C_s$, where C_s is the capacitance of the segment, and Q_0 is the equilibrium value of the charge, determined by V_G. Because the charge is quantized, however, this gives rise to an activation energy of $e^2/2C_s$ for adding an extra electron to the segment when Q_0 corresponds to an integer multiple of e, but no activation energy when Q_0 corresponds to a odd multiple of $e/2$. It is implicitly assumed that the single-particle energy splittings are negligible compared to the Coulomb energy. Thus, the conductance, its activation energy, and the threshold for non-Ohmic behavior are expected to oscillate with the number of electrons on the isolated segment. This model predicts that L_0 is the length of the isolated segment.

The CB model predicts that the activation energy ΔE at conductance minima, the gate-voltage spacing ΔV of the conductance peaks, and the threshold voltage V_t in the I-V_{DS} curve at the minima are all related in a simple way: $\Delta E = e\,\Delta V/2 = eV_t = e^2/2C_s$. In our Si device the capacitance C_s is dominated by that between the channel and the lower gate, and ΔV is therefore the frequency measured when the lower-gate voltage is varied. We found $V_t = 0.7$ meV for several of the minima in Fig. 12, and $\Delta V = 1.9$ meV. For this case, the agreement with the CB prediction is good, given that the criterion for determination of V_t is somewhat arbitrary. However, as illustrated in Fig. 16, ΔV does not scale with ΔE.

There are several additional qualitative deficiencies of the CB model. First, the usual assumption in this model is that the single-particle levels in the isolated segment may be taken to be a continuum. This is certainly adequate when applying the CB model to metallic particles in an insulating matrix. However, for the devices under consideration here, a simple calculation shows that for $L_0 \sim 1$ μm the single-particle energy spacings are comparable to the measured activation energies at densities of $\sim 10^6$ cm^{-1} electrons, assuming that the energies go as k^2. Second, because of the degeneracies discussed above, the activation energies would equal $e^2/2C_s$ when the Fermi energy coincides with degenerate single-particle levels, but would be larger by the single-particle-level splittings when it is between sets of degenerate levels. Third, the application of a magnetic field would increase the former activation energies and reduce the latter ones by lifting the spin degeneracy. This would be seen as a modulation of the conductance minima in an experiment like that of Fig. 19. We have searched carefully for such an effect and have not seen it. Last, one expects to observe the "Coulomb staircase," a series of equal steps in the I-V_{DS} curve, because a new conductance channel opens up whenever V_{DS} increases enough to add another electron to the isolated segment. Most of these deficiencies are common to the CB model and the noninteracting resonant-tunneling model discussed above.

C. Charge-density wave

The calculation of Laux and Stern[9] suggests that for the densities at which the oscillations are observed, only a few subbands are occupied for motion transverse to the narrow channel. In the lowest subband, because the system is dynamically one dimensional, the system is expected to be unstable relative to the formation of a spin- or charge-density wave (CDW).[12] Indeed, the condition for the formation of a Wigner crystal,[13] that the zero-point energy is less than the Coulomb interaction, is satisfied for most of the density range in which the conductance oscillates.

We have therefore proposed[3,4] that the electrons in our narrow channels form a CDW and that the pinning of this CDW by interface charges gives rise to the oscillatory and non-Ohmic behavior that we observe. To test whether this is consistent with our observations, we have followed the approach of Teranishi and Kubo,[14] who

used the model Hamiltonian of Lee, Rice, and Anderson[15] and of Fukuyama[16] to model the CDW. In this model, the charge density $\rho(x)$ takes the form $\rho(x)=\rho_0\cos[Qx+\phi(x)]$, where $Q=2\pi/\lambda=2\pi n$ is the wave vector of the CDW. It is assumed that amplitude variations are energetically much more costly than phase variations, so that $\phi(x)$ takes into account any deformations caused by external perturbations. The CDW is further characterized by an elastic deformation constant and an effective mass density. The elastic deformation characterizes the electron-electron repulsion, which was only treated in an average way in the CB model discussed above.

Teranishi and Kubo[14] studied the case where a CDW with the above form for $\rho(x)$ interacts with a number of randomly placed δ-function impurities. To investigate our system, we have extended their model in two ways. First, we examined the solutions of the model as Q was varied, which is analogous to varying the gate voltage. Second, we included the effect of varying the *strengths* of the δ-function impurities, since in the real system the impurity potentials have varying magnitudes.

To get an idea of what the true impurity potential "seen" by an electron might look like, we performed the following computer simulation: We randomly sprinkled 10^{10} cm^{-2} Coulomb impurities on a two-dimensional plane, and extracted the potential energy along a 10-μm-long (one-dimensional) line. A typical plot of the random potential generated in this way is shown in Fig. 24 (top panel). One can see that only a few impurities contribute strongly to the potential, and that, in this example, one can pick out three dominant impurities which define two lengths, L_1 and L_2. As explained in Ref. 3, a length L_0 between two impurities will lead to oscillations of the pinning energy, and thence of the conductance, with period $\Delta Q=2\pi/L_0$. The impurity arrangement in Fig. 24 might thus be expected to lead to two superimposed periods, with periods $2\pi/L_1$ and $2\pi/L_2$.

To test this supposition, we ran a simulation of the model of Teranishi and Kubo; when using this model we replaced the sharp potential valleys of Fig. 24 by δ functions of proportional height. These δ functions are shown at the bottom of Fig. 24. The absolute height of the δ functions to be used in this model depends on the ratio of an impurity's coupling to the CDW to the elastic energy of the wave itself. Since both these energies are Coulombic in nature, we expect this ratio to be of order unity. The result of such a simulation is shown in Fig. 25. The top panel shows the total energy of the CDW as $Q=2\pi n$ is varied. The range of Q shown corresponds to gate voltages in the MOSFET from about 0.4 to 0.6 V above threshold. One can clearly see a short-period oscillation with $\Delta Q\sim 9\ \mu\text{m}^{-1}$; the longer period is difficult to pick out by eye. The bottom panel of Fig. 25 shows a power Fourier transform of the energy versus Q, taken over a larger range of Q than shown in the top panel. Here both periods are clearly visible. The important lengths obtained from $L_0=2\pi/\Delta Q$, which corresponds to $L_0=0.7$ and 2.75 μm, are shown in Fig. 24. This simulation clearly shows how the distance between impurities directly determines the period of the oscillations. It also shows how, if there are more than one pair of impurities

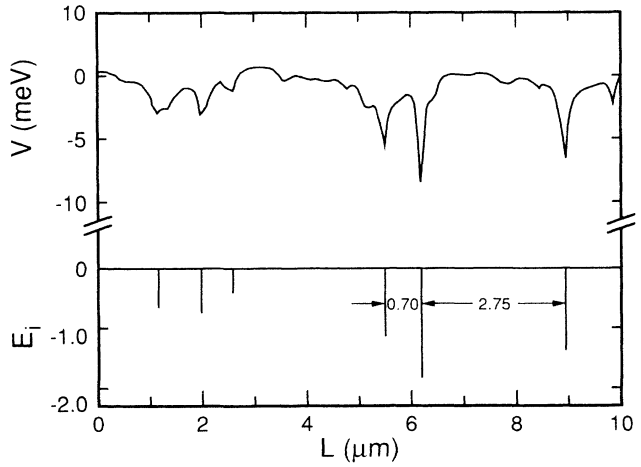

FIG. 24. Top panel: simulation of the potential along a 10-μm-long wire embedded in a two-dimensional plane of Coulombic charges (see text). The potential is generally smooth with occasional sharp dips when an impurity lies near the channel. Bottom panel: the model potential used in the simulation of the theory of Ref. 14. The more realistic potential in the top panel is modeled by six δ functions. The distances in μm between the three strongest impurities are shown.

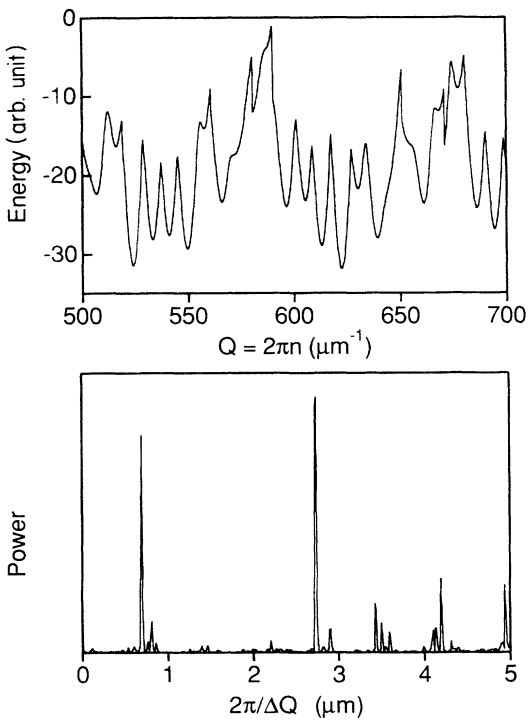

FIG. 25. Top panel: the energy of a pinned CDW is shown as a function of the wave number or electron density, as derived using the model described in the text. Two periods are visible in these data. Lower panel: the Fourier transform of the above clearly shows the two periods, corresponding to the two "important" distances between impurities shown in Fig. 24.

lying close to the channel, one may get more than one period at once, as is, in fact, often observed in the experiments.

The simulation calculates the ground-state energy for any Q, and this energy is found to oscillate periodically in Q. Exactly how this periodic behavior in the pinning energy leads to a periodic conductance is not clear. We have seen that the conductance is activated, except at the lowest temperatures. This suggests that conduction proceeds in this regime via thermal activation over a barrier. In the CDW model this barrier would be the total CDW energy, and hence we associate the ground-state energies calculated above with the thermal activation energies measured experimentally; a comparison of Figs. 15 and 25 shows that the behavior is similar. In the temperature regime where tunneling appears to be important, the total energy of the CDW will determine the tunneling rate. The many-body CDW state must tunnel in a collective manner across an energy barrier, and again the relevant barrier is the difference in total energies between the states with one electron added or subtracted.

The CDW model may also explain the threshold behavior in the I-V_{DS} dependence. The classical washboard potential model[17] predicts that the current above threshold should follow

$$I/V = G_0[1-(V_T/V)^2]^{1/2}, \tag{1}$$

where G_0 is a constant. In Fig. 26 we compare this prediction with experiment and find reasonable agreement. The sketch in the inset illustrates the classical behavior following Grüner.[17]

To explain the independence of the frequency of oscillations on magnetic field, one must assume that the CDW is in the Wigner-crystal limit in which, because of the strong correlations, the spin degeneracy is irrelevant. The temperature dependence of the conductance is yet to be modeled in detail. Since charge transport requires that an extra charge be added to the region between the pinning centers, the thermally activated mechanism may turn out to be quite similar to that in the CB model. However, for the CDW the strength of the pinning will also play a role, and this may account for the variability of the activation energy seen, for example, in Fig. 15. The tunneling component of the conductance might result from a mechanism like that of Larkin and Lee.[18]

One additional attractive feature of the CDW model is that the pinning centers can be positively or negatively charged, whereas the CB and noninteracting resonant-tunneling models require repulsive potentials to isolate the segment of the channel. As noted above, the majority of the interface charges in the Si devices are positively charged, and thus attractive for electrons. Of course, there will be a minority of negative charges, and these may be sufficient to create barriers.

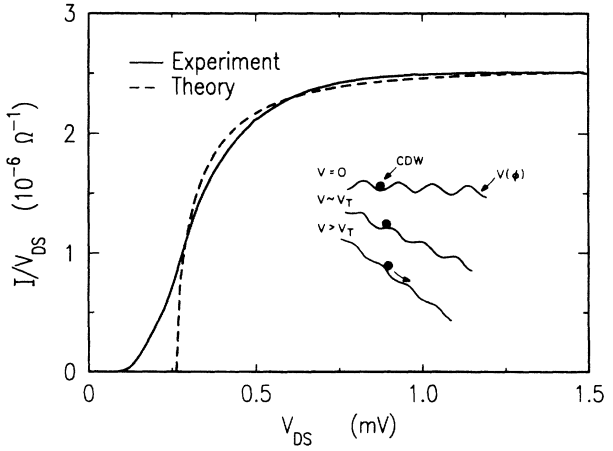

FIG. 26. Current divided by the applied voltage vs V_{DS} in a minimum is compared with a least-squares fit to the behavior predicted by the classical model [Eq. (1)]. The inset [after Grüner (Ref. 17)] shows the mechanism of depinning the charge-density wave as the applied voltage is increased. $V(\phi)$ is the pinning potential created by the impurities. V_{DS} is the applied source-drain voltage, and V_T the threshold voltage.

VI. CONCLUSIONS

The periodic conductance oscillations are a very surprising phenomenon. We have presented a strong case that the period reflects a length that is determined by the distance between interface charges that fall close to the conducting channel. While we cannot say with certainty what the length per electron L_0 corresponds to, the observation of high frequencies, with values of L_0 comparable to the channel length, strongly suggests that each cycle corresponds to the addition of a single electron to the region between the interface charges.

While the oscillations are fairly universal, having been now observed in Si n- and p-type layers and GaAs n-type layers, it is apparent that moderately clean and narrow channels are required. Obviously, even if the periodic oscillations persist in dirtier channels, when the number of impurities is large, the number of frequencies will be too, and periodicities will be hard to identify. Narrow channels are required to reduce the dimensionality in the CDW model and to reduce the capacitance in the CB model.

The two models that do best at explaining the phenomena are the CB and CDW models in which the periodicity arises from the Coulomb interaction between electrons. While the CDW, because it includes correlations, has some advantages over the CB model, it appears that disorder may need to be included at an early stage in the modeling.[19] It is known[20] that the strong interacting one-dimensional Fermi gas has a complicated phase diagram when disorder is included, and the location of our devices in that diagram is still uncertain.

ACKNOWLEDGMENTS

We are grateful to N. Wingreen and P. A. Lee for stimulating discussions; to T. Yen, J. Carter, and S. Park

for help in Si process development; to M. Heiblum and H. Shtrikman and to Mark Shepard for essential GaAs sample growth; and to the Focused Ion Beam group at the Massachusetts Institute of Technology for help in x-ray mask fabrication. This work was supported by the U.S. National Science Foundation under Grant No. ECS-88-13250 and by the U.S. Joint Services Electronics Program under Contract No. DAAL03-89-C-0001.

---

*Present address: Department of Physics, University of Michigan, Ann Arbor, MI 48109-1120.

[1]See, for example, A. D. Stone, Phys. Rev. Lett. **54**, 2692 (1985).

[2]B. L. Alt'shuler, Pis'ma Zh. Eksp. Teor. Fiz. **41**, 53 (1985) [JETP Lett. **41**, 648 (1985)]; P. A. Lee and A. D. Stone, Phys. Rev. Lett. **55**, 1622 (1985); M. A. Kastner, R. F. Kwasnick, J. C. Licini, and D. J. Bishop, Phys. Rev. B **36**, 8015 (1987).

[3]J. H. F. Scott-Thomas, S. B. Field, M. A. Kastner, H. I. Smith, and D. A. Antoniadis, Phys. Rev. Lett. **62**, 583 (1989).

[4]U. Meirav, M. A. Kastner, M. Heiblum, and S. J. Wind, Phys. Rev. B **40**, 5871 (1989).

[5]J. H. F. Scott-Thomas, M. A. Kastner, D. A. Antoniadis, H. I. Smith, and S. B. Field, J. Vac. Sci. Technol. B **6**, 1841 (1988).

[6]U. Meirav, M. Heiblum, and F. Stern, Appl. Phys. Lett. **52**, 1268 (1988).

[7]A. B. Fowler, A Hartstein, and R. A. Webb, Phys. Rev. Lett. **48**, 196 (1982); C. C. Dean and M. Pepper, J. Phys. C **15**, L1287 (1982); A. Ya. Shik, Fiz. Tekh. Polyprovodn, **19**, 1488 (1985) [Sov. Phys.—Semicond. **19**, 915 (1985)].

[8]M. R. Pinto, C. S. Rafferty, and R. W. Dutton, Computer Code PISCES-II (Stanford Electronics Laboratories, Stanford University, Stanford, CA 94305).

[9]S. E. Laux and F. Stern, Appl. Phys. Lett. **49**, 91 (1986).

[10]T. P. Smith *et al.*, Phys. Rev. Lett. **61**, 585 (1988).

[11]K. K. Likharev, IBM J. Res. Develop. **32**, 144 (1988), and references therein; M. Amman, K. Mullen, and E. Ben-Jacob, J. Appl. Phys. **65**, 339 (1989); H. Van Houten and C. W. J. Beenakker, Phys. Rev. Lett. **63**, 1893 (1989).

[12]See, for example, J. B. Torrance, in *Chemistry and Physics of One Dimensional Metals,* edited by Heimo J. Keller (Plenum, New York, 1976), pp. 137–166, and references therein.

[13]See, for example, N. F. Mott and E. A. Davis, *Electronic Process in Non-Crystalline Materials* (Oxford University Press, London, 1989).

[14]N. Teranishi and R. Kubo, J. Phys. Soc. Jpn. **47**, 720 (1979).

[15]P. A. Lee, T. M. Rice, and P. W. Anderson, Solid State Commmun. **14**, 703 (1974).

[16]H. Fukuyama, J. Phys. Soc. Jpn. **41**, 513 (1976).

[17]See, for example, G. Grüner, Rev. Mod. Phys. **60**, 1129 (1988).

[18]A. I. Larkin and P. A. Lee, Phys. Rev. B **17**, 1596 (1978).

[19]N. W. Wingreen and P. A. Lee (private communication).

[20]W. Apel and T. M. Rice, Phys. Rev. B **26**, 7063 (1982); T. Giamarchi and H. J. Schulz, *ibid.* **37**, 325 (1987).

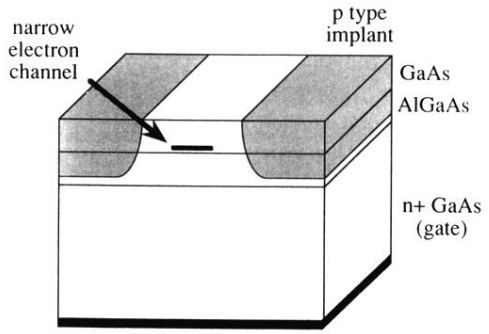

FIG. 2. Schematic of the GaAs device, which is an inverted heterojunction structure in which the density of electrons is controlled by the degenerate n-type GaAs gate. The electrons are confined laterally by acceptors implanted in the GaAs and $Al_xGa_{1-x}As$ layers.